PAPER

Check for updates

Synthesis, characterization, antimicrobial and antibiofilm potential of green copper silicate and zinc silicate nanoparticles: kinetic study and reaction mechanism determination

Ashraf A. Qurtam, [ID] [a] Ibrahim Elbatal, [ID] [b] Fahd A. Nasr, [ID] [a] Ashraf A. Elgendy, [ID] [c] Gharieb S. El-Sayyad [ID] *[d] and Ahmed I. El-Batal [ID] [e]

The study explored an eco-friendly method to synthesize Cu silicate and zinc silicate nanoparticles (NPs) and characterize them using analytical instruments like transmission electron microscopy, DLS analysis, Zeta potential, EDX elemental analysis, and scanning electron microscopy with mapping. We tested how well Cu silicate and Zn silicate NPs can fight bacteria that cause wound infections and unicellular pathogenic fungi by checking their antimicrobial properties, the smallest amount needed to stop growth (minimum inhibitory concentration), and their ability to prevent biofilm formation. To investigate a potential mechanism of antimicrobial behavior, we applied the membrane leakage experiment. The generated Cu silicate and Zn silicate NPs have shown promising antimicrobial activity against all investigated bacteria and unicellular fungi. The MIC was calculated at a concentration of 39.062 μg mL^{-1}, and Cu silicate NPs created ZOI at a 27.0 mm where *S. aureus* could not grow, additionally Cu silicate NPs produced a 25.0 mm ZOI against *C. albicans* and MIC was 19.53 μg mL^{-1}, and a 19.0 mm ZOI against *E. agglomerans* and MIC was 19.53 μg mL^{-1}. *S. aureus* is more affected by Zn silicate NPs, showing a 41.0 mm ZOI and MIC was calculated at 19.53 μg mL^{-1}, followed by *C. albicans* with a 30.0 mm ZOI at 9.765 μg mL^{-1}, *E. agglomerans* with a 29.0 mm ZOI and MIC at 39.062 μg mL^{-1}, and *S. epidermidis* with a 28.0 mm ZOI at 19.53 μg/mL MIC. However, the promising results were obtained for *K. pneumoniae* (26.0 mm ZOI, 9.765 μg/mL MIC), *P. aeruginosa* (25.0 mm ZOI, 9.765 μg/mL MIC), and *E. coli* (21.0 mm ZOI, 19.53 μg/mL MIC). As a new era for combating some diseases' resistance in the biomedical areas, the encouraging results indicated that the generated nano-formula should be used against the harmful bacteria.

1 Introduction

Serious health problems have lately arisen as a result of pathogen (viruses, fungi, and bacteria) resistance to conventional antimicrobial therapy.[1] Currently, the entire community is fighting an invisible infectious agents to stop the spread of illnesses and preserve lives.[2,3]

Researchers have developed self-cleaning surfaces to prevent hospital infections, prevalent hospital-associated illnesses, and the growth of bacteria resistant to new therapies.[4] Long-term antibacterial activity is a highly desirable feature that remains appealing while ensuring cytocompatibility.[5]

The scientific field of nanotechnology has broad applications across numerous fields. Because of their narrow particle size, large surface area, and distinctive morphological characteristics, nanoparticles (NPs) differ from conventional substances.[6–10] Recent developments in the application of nanotechnology have made it easier to synthesize nano-sized particles with potential medical uses.[11] Because nanoparticles have natural antibacterial qualities, especially metal nanoparticles, many new antimicrobial materials have been developed using them.[12,13] The antibacterial properties of nanoparticles, particularly metal nanoparticles, have led to the creation of various nanomaterials based on NPs.[14]

The antibacterial effects of ZnO NPs, and CuO NPs have been widely studied because they work better than traditional

[a]Biology Department, College of Science, Imam Mohammad Ibn Saud Islamic University (IMSIU), Riyadh, 11623, Saudi Arabia

[b]Department of Mathematics and Statistics, College of Science, Imam Mohammad Ibn Saud Islamic University (IMSIU), Riyadh, 11623, Saudi Arabia

[c]Department of Immunology, New Kasr Al-Aini Teaching Hospital, Cairo, Egypt

[d]Department of Medical Laboratory Technology, Faculty of Applied Health Sciences Technology, Badr University in Cairo (BUC), Badr City, Cairo, Egypt. E-mail: Gharieb.El-Saied@buc.edu.eg

[e]Drug Microbiology Lab., Drug Radiation Research Department, National Center for Radiation Research and Technology (NCRRT), Egyptian Atomic Energy Authority (EAEA), Cairo, Egypt

antimicrobial treatments. In addition to having a longer shelf life, these nanoparticles are reusable, more stable over a wider range of temperatures and pressures, and comparatively easy to store and transport.[15] Numerous factors, such as size, shape, strength, purity, structural flaws, and exposure level, have been linked to the antibacterial potential of ZnO and CuO NPs.[16] To function as antimicrobials, ZnO NPs, and CuO NPs must first produce reactive oxygen species (ROS),[17] then disrupt cell membranes, be absorbed by cells, physically injure cells, and release toxic levels of zinc ions.[18–21] Combining ZnO, and CuO NPs with rare earth elements and transition metals (like Ag) increased its antibacterial activity. Defects such as oxygen and zinc vacancies that occurred in the treated ZnO NPs might have caused this result.[22,23] The antioxidant and antibacterial qualities of ZnO NPs loaded with Fe and Al have been studied by Verma *et al.*[24]

Nanoparticles of zinc silicate and copper silicate have attracted a lot of interest because of their potential uses in various industries, such as electronics, coatings, and catalysis. Mixing silicate with copper or zinc creates these nanoparticles, resulting in materials with unique qualities. Zinc silicate NPs can be synthesized *via* various techniques, such as the reaction of zinc acetate with tetrabutylammonium hydroxide in the presence of a glass wall, which produces willemite Zn_2SiO_4 microcrystals and films and hemimorphite $Zn_4Si_2O_7(OH)_2 \cdot nH_2O$.[25] On the other hand, copper silicate nanoparticles can be made by mixing sodium silicate and cuprous oxide, resulting in a coating that helps prevent unwanted growth.[26]

There are several possible uses for copper silicate and zinc silicate NPs.[27] For example, because of their high surface area and porous nature, zinc silicate NPs can be utilized as catalytic supports.[28] Because of their antifouling qualities, copper silicate NPs can be used in coatings to stop marine organisms from growing on surfaces.[29] Additionally, research has looked into using copper oxide and zinc oxide NPs as pigments in paint that can resist heat and corrosion, showing promising results in enhancing how well the coatings work.[30]

By adding copper silicate and zinc silicate NPs, coating properties can be significantly enhanced. For example, it has been shown that incorporating ZnO NPs and CuO NPs into silicon resin paints improves their ability to tolerate heat and inhibit corrosion.[30,31] The way these NPs are spread out in the coating is important for achieving the best performance because it affects how well the coating protects and lasts over time.

Nanoparticles of zinc silicate and copper silicate show promise and have prospective uses in several industries, including as coatings and catalysis.[32] Their performance in various applications is largely determined by their synthesis techniques and properties. To fully investigate their potential and maximize their application across a range of industries and biomedical applications, more research is required.

Our research offers a simple, environmentally friendly method to create new Zn silicate and Cu silicate NPs that can enhance their stability and reactivity in biological applications. Therefore, this combination opens new possibilities for their potential usage as antimicrobial agents against specific pathogenic microbes.

2 Material and methods

2.1. Chemical and reagents

Oxoid and Difco provided the media components employed in microbiological experimental investigations. Every chemical and reagent employed in this investigation was of analytical quality. The study's nanoparticle synthesis used gum Arabic, copper sulphate, sodium silicate and zinc sulphate, which were purchased from Sigma-Aldrich in the United Kingdom.

2.2. Synthesis of zinc silicate and copper silicate NPs

To create Cu silicate and Zn silicate NPs using the green approach, 20 grams of gum Arabic were dissolved in 700 milliliters of distilled water. Ten grams of sodium silicate were then added to the gum Arabic solution, stirred at 600 rpm, and heated to 50 °C for approximately two hours. Following that, 11 grams of copper sulfate pentahydrate ($CuSO_4 \cdot 5H_2O$) were dissolved in 200 milliliters of distilled water to create the solution (A), and 12 grams of zinc sulphate heptahydrate ($ZnSO_4 \cdot 7H_2O$) were dissolved in 200 milliliters of distilled water to create the solution (B). This solution (A, and B) was separately then added drop-by-drop to the final gum Arabic-sodium silicate solution while being stirred at 600 rpm and heated to 50 °C for around an hour. After checking and adjusting the pH with an acetic acid solution to about 6.5, the resultant solution was filled to 1000 mL and heated to 50 °C for approximately an hour. The color shift indicated the generation of green Cu silicate and Zn silicate NPs.

2.3. Characterization of zinc silicate and copper silicate NPs

A high-resolution transmission electron microscope (HR-TEM, JEM2100, Jeol, Japan) was used to check the size and shape of the Cu silicate and Zn silicate nanoparticles, while a scanning electron microscope (SEM, ZEISS, EVO-MA10, Germany) was used to look at the surface's shape and structure. A facility located in St. Barbara, California, USA, utilized dynamic light scattering with the DLS-PSS-NICOMP 380-ZLS equipment to measure the average size of the generated Cu silicate and Zn silicate nanoparticles. Finally, a zeta potential analyzer from Malvern Device, UK, was used to randomly check the surface charges of the created Cu silicate and Zn silicate nanoparticles at the pH level they were made. The measurements were carried out in triplicate ($n = 3$).

2.4. Antimicrobial activity of zinc silicate and copper silicate NPs

Various harmful bacteria, such as *Escherichia coli*, *Pseudomonas aeruginosa*, *Klebsiella pneumoniae*, *Enterobacter agglomerans*, *Staphylococcus epidermidis*, *Staphylococcus aureus*, and the yeast *Candida albicans*, were tested for assess the potential antimicrobial activity of the synthesized NPs using the agar well diffusion method.[33]

Bacterial suspensions that had been adjusted to 0.5 McFarland standards were inoculated overnight into plates that contained nutrient agar medium. All plates were incubated overnight at 37 °C following the use of nystatin as an antifungal agent and streptomycin (S10 μg mL^{-1}) as a positive control antibiotic (antibacterial agent). The inhibitory zones' diameter was measured in millimeters after the plates were incubated.

2.5. Minimum inhibitory concentration (MIC) determination

The Cu silicate and Zn silicate nanoparticles were tested to find out the lowest amount needed to stop the growth of bacteria using a method called serial dilution.[34] In these instances, Mueller Hinton (MH) broth and the tested NPs (Cu silicate and Zn silicate NPs) were included in a negative test, while MH and the same microbe were included in a positive test. At 37.0 ± 2 °C, the MIC was measured during the incubation period. Bacterial inoculums were generated at 3–6 × 10^7 CFU mL^{-1}, while unicellular fungi were maintained at 2–4 × 10^7 CFU mL^{-1}. The ELISA plate method was used to measure MIC at 600 nm.

2.6. Antibiofilm activity of the synthesized zinc silicate and copper silicate NPs

We assessed the effectiveness of Cu silicate and Zn silicate NPs (19.53 μg mL^{-1}; MIC) in limiting the growth of sensitive bacteria compared to the control sample by visually examining the biofilm that formed at the tube's surface with and without these NPs. This semi-qualitative evaluation of biofilm generation was investigated in the Christensen *et al.* study.[35] The bacteria and *Candida* sp. under investigation were introduced to each tube along with 5.0 mL of MH broth following a 0.5 McFarland calibration. After the contents of the tubes were carefully removed, the resultant solution was incubated for overnight at 37.0 ± 2 °C. Following a ten-minute treatment with a 3.0% sodium acetate solution, deionized water was used to rinse the connected bacterial layers. The bacterial biofilms were then colored using 0.1% crystal violet (CV). Using a UV-visible spectrometer setup to detect light at 570.0 nm, the percentage of microbial biofilms was examined. Using eqn (1).

$$\text{Inhibition biofilm percentage (\%)} = (\text{O.D. of control sample} \\ - \text{O.D. of the treated sample})/ \\ (\text{O.D. of control sample}) \times 100 \quad (1)$$

2.7. Growth curve assay

Following Huang *et al.*,[36] we studied how Cu silicate and Zn silicate NPs affect the growth of *C. albicans*, *S. epidermidis*, and *P. aeruginosa* by using a growth curve experiment. We added 0.5 McFarland (1 × 10^8 CFU mL^{-1}) cultures of bacteria and yeast to 5.0 mL nutrient broth tubes and then added equal and different amounts of Cu silicate and Zn silicate NPs to each tube we were testing. It must be noted that, 0.5 McFarland (1 × 10^8 CFU mL^{-1}) bacterial and yeast cultures were added to 5.0 mL nutrient broth tubes. Equal and different amounts of Cu silicate and Zn silicate NPs were added to each tube under examination. At intervals of 0.0, 2.0, 4.0, 6.0, 12.0, and 24 hours until 24 hours after treatment, the absorbance of bacterial and yeast growth was determined. A UV-visible spectrophotometer was used to measure the samples' optical density at $\lambda = 600$ nm. The typical growth curve was created by comparing the average duplicate data at hourly intervals.

2.8. The NPs' impact on microbial protein permeability

The Cu silicate and Zn silicate nanoparticles were combined with 10 mL of nutrient broth after counting the test microorganisms at 1 × 10^8 CFU mL^{-1} for 18 hours. Solutions without the NPs were given to the control group. The samples were spun in a centrifuge for 10 minutes at 5000 rpm after being incubated for 5 hours at 37 °C. Culture-mixed solutions without NPs were administered to the control group. The samples were centrifuged for 10 minutes at 5000 rpm following a 5-hour incubation period at 37 °C. The 100 μL of supernatant that was extracted from the examined samples was combined with 1 mL of Bradford reagent. Optical density was measured at 595 nm following a 10-minute dark incubation period.[37]

2.9. Statistical analysis

To determine the statistical analysis of the obtained results, a one-way ANOVA (at $P < 0.01$) was performed and organized in accordance with Duncan's multiple sequence analyses.[38] SPSS software, version 15, was utilized for data evaluation and analysis.

3 Results and discussion

3.1. Characterization of the synthesized Cu silicate and Zn silicate NPs

3.1.1. HRTEM and SEM-EDX mapping imaging. HRTEM imaging analysis was conducted to show the size and form of the produced Zn silicate and Cu silicate NPs. Fig. 1a shows that the produced Cu silicate NPs has a round shape and is uniform in size and possessed an average diameter of 74.23 ± 1.0 nm (Fig. 1b). The synthesized Zn silicate NPs had a round shape (Fig. 1c) and an average diameter of 71.12 ± 1.2 nm (Fig. 1d).

According to a review of common particle size and shape in existing studies, Castro-Longoria *et al.*,[39] used an extract from a filamentous fungus to create silver, gold, and silver-gold bimetallic materials, with a comparison in the NPs sized in our study, the synthesized Zn silicate and Cu silicate NPs were in the nanoscale and primarily spherical which increasing their catalytic potential specially as a smart antimicrobial agents. When the fungus was subjected to aqueous solutions of 10^{-3} M of AgNO$_3$ and HAuCl$_4$, respectively, the NPs were observed to be predominantly spherical in shape. It was found that the average diameters of the NPs for silver and gold were 11.0 nm and 32.0 nm, respectively.

Although diverse morphologies may be observed due to the artificial manner of the extract, the anisotropic shape had been documented. The extracted NPs' shapes were generally round or
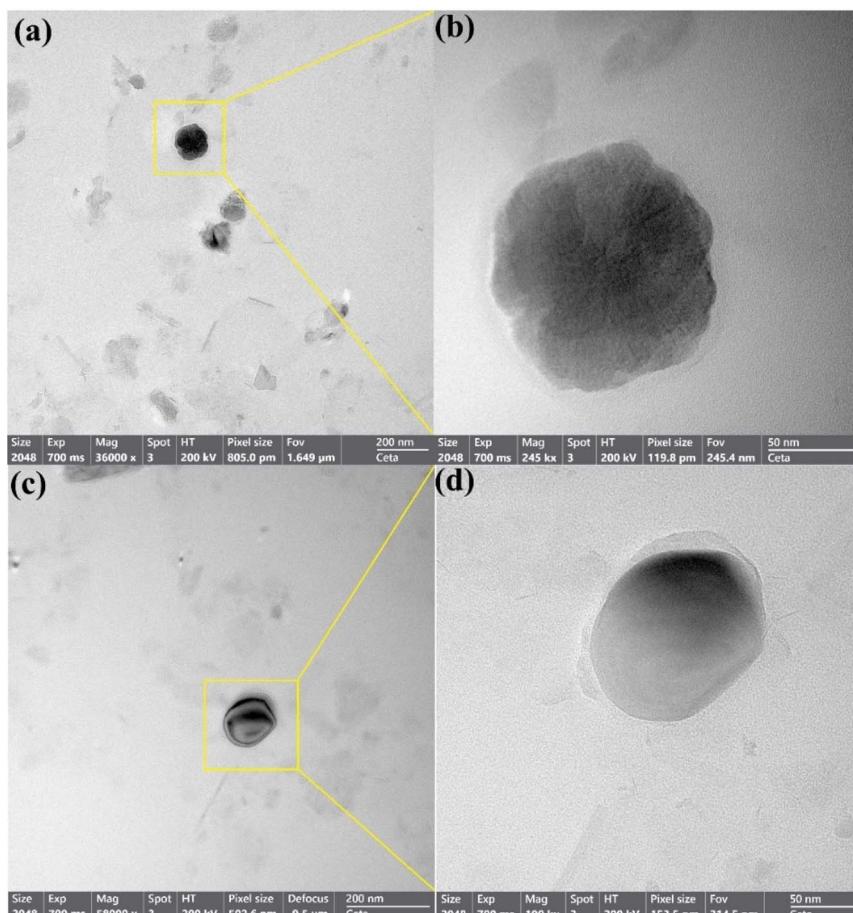
Fig. 1 HRTEM imaging of the synthesized Cu silicate NPs (a and b), and Zn silicate NPs (c and d).

elliptical in all instances; thus, the forms created in that study,[39] may vary. In our experiment, we used only one reduction and capping agent (Gum Arabic), resulting in consistent shape.

Furthermore, we examined the shape and surface properties of the generated silicate NPs using SEM. Fig. 2a displays the generated Cu silicate NPs as a single, bright, rounded particle. We investigate the surface shape and elemental composition of Cu silicate NPs using EDX graphs and images from scanning electron microscopy. The SEM image in Fig. 2a shows that the Cu silicate NPs have a smooth, round shape, which is similar to what was found in earlier studies.[27] The Cu silicate NPs have a complicated structure and are consistently sized. The EDX mapping of the nanoparticles confirmed the creation of Cu silicate NPs by showing that Cu, O, and Si are evenly spread out (Fig. 2b).

The synthesized Zn silicate NPs are finally shown in Fig. 3a as solitary, rounded, and brilliant particles. EDX graphs and scanning electron microscopy pictures are used to analyze the surface shape and elemental makeup of Zn silicate nanoparticles. Fig. 3a shows the SEM image of Zn silicate nanoparticles with a uniform, spherical surface, which is similar to the shape seen in the published studies.[40] Zinc silicate NPs have a complicated structure and are consistently sized. The EDX mapping of the nanoparticles showed that Zn, O, and Si are

evenly spread out, confirming that Zn silicate NPs have formed (Fig. 3b).

3.1.2. DLS analysis and zeta potential. According to Fig. 4, the DLS method found that the particle size for Cu silicate and Zn silicate nanoparticles made with gum Arabic was 219.4 ± 2.0, and 192.0 ± 1.7 nm, respectively (Fig. 4a and b).

According to the International Standards Organizations (ISOs), samples are considered monodispersed if the polydispersity index (PDI) readings are less than 0.05. However, if the PDI findings are greater than 0.7, it indicates that the particles are of varying sizes. According to the International Standards Organizations (ISOs), samples are deemed monodisperse if the polydispersity index (PDI) readings are less than 0.05. The particles have a diverse size distribution; nevertheless, if the PDI findings are higher than 0.7. The samples are classified as monodisperse by the International Standards Organizations (ISOs) if the polydispersity index (PDI) findings are less than 0.05. However, we should produce particles with a varied distribution when the PDI results are above 0.7.[41] According to our findings, the PDI values of the Cu silicate and Zn silicate NPs that were generated were 0.86 and 0.81, respectively. According to the current results, the generated Cu silicate and Zn silicate NPs displayed an acceptable range of polymorphism.[42] The findings showed that the average particle sizes
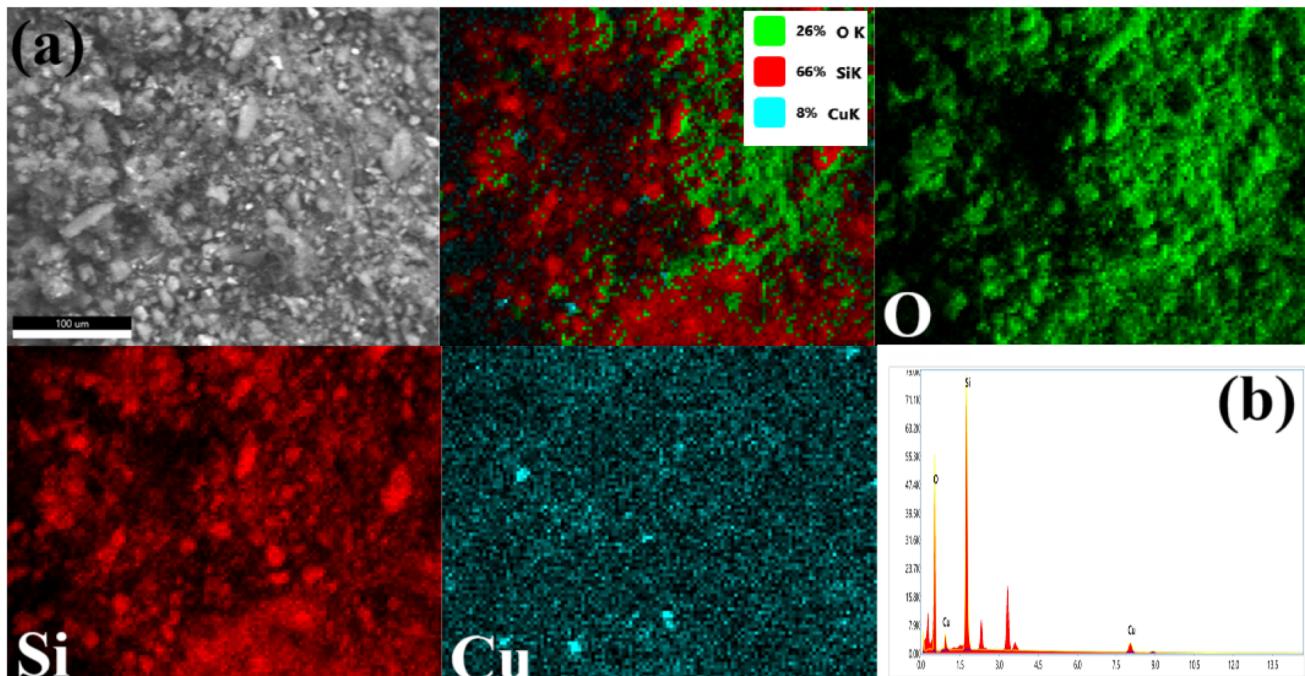
Fig. 2 SEM mapping images (a), and EDX analysis (b) of the synthesized Cu silicate NPs.

determined by DLS analysis were larger than the particle sizes determined by HR-TEM imaging. According to ref. 43, the hydrodynamic radius of the generated Cu silicate and Zn silicate NPs and the water surrounding their layers is responsible for the remarkable diameters of the developed NPs.

The procedure can significantly affect the PSD results since every measurement strategy has a unique set of principles and sensitivities. Sieve method,[44] laser diffraction,[45] DLS,[46] microscopy,[47] and sedimentation[48] are some significant methods by which this may happen. Each strategy has pros and cons of its own, and the method employed may have a significant effect on
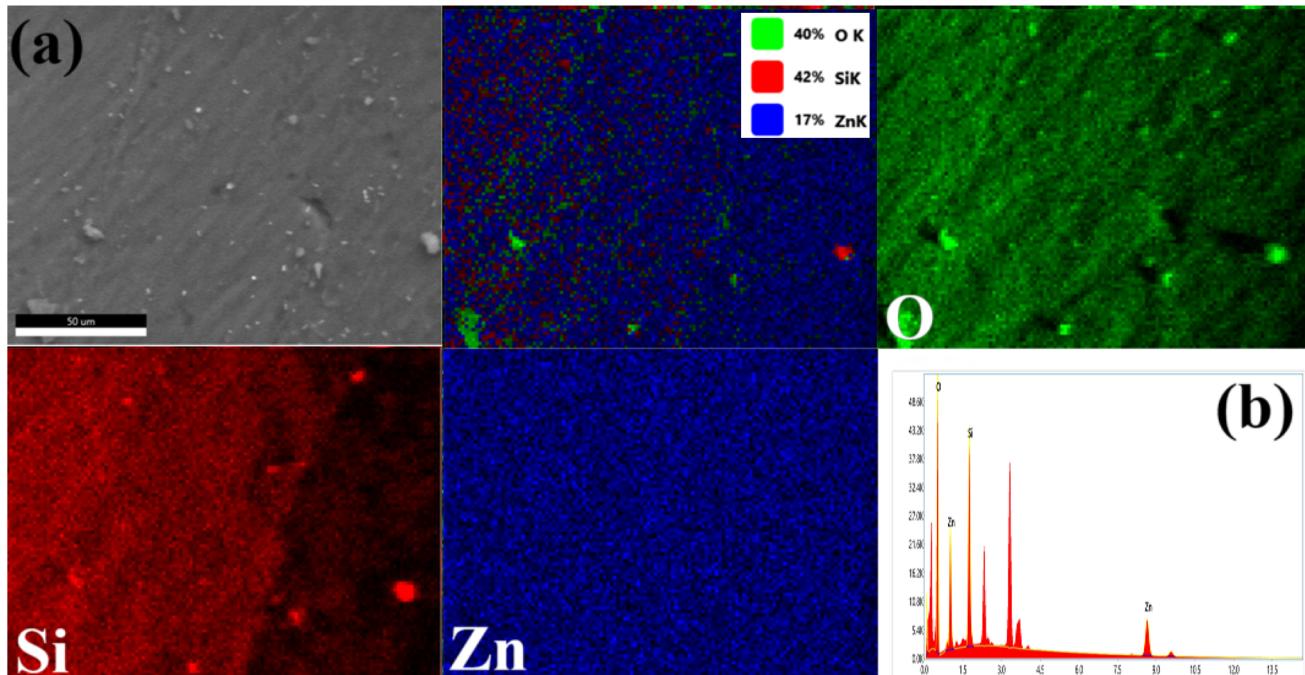

Fig. 3 SEM mapping images (a), and EDX analysis (b) of the synthesized Zn silicate NPs.
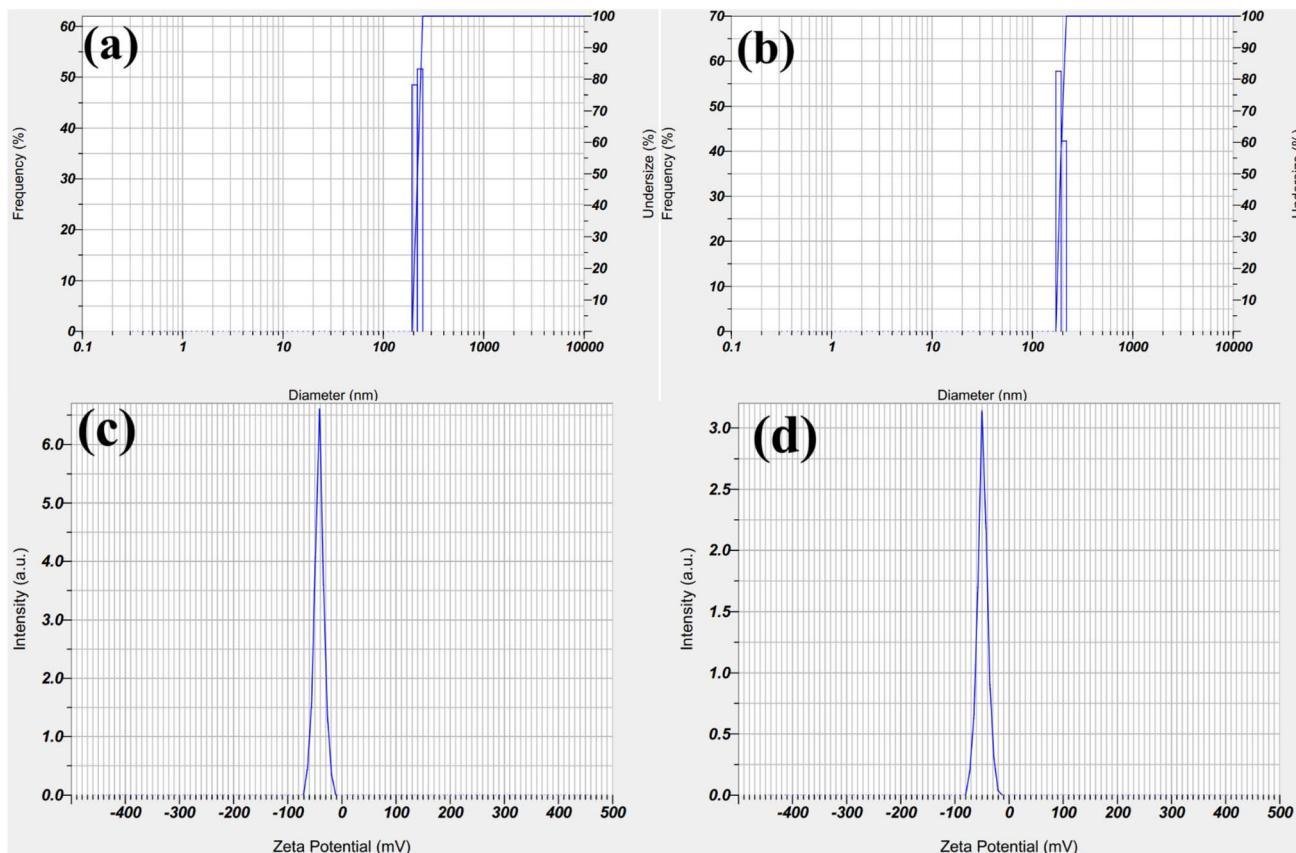
Fig. 4 Particle size distribution, and surface charge of the synthesized Cu silicate and Zn silicate NPs where (a) DLS analysis of Cu silicate NPs, (b) DLS analysis of Zn silicate NPs, (c) zeta potential of Cu silicate NPs, and (d) zeta potential of Zn silicate NPs (they were performed in triplicate ($n = 3$)).

the reported PSD levels. A variety of approaches are frequently useful in order to fully comprehend the particle size distribution.

As shown in Fig. 4c and d, the zeta potential of the Cu silicate and Zn silicate nanoparticles was measured during their preparation at a pH of 6.5. The current results indicate that the zeta potential of the Cu silicate and Zn silicate NP interactions remain negative at the substance's pH throughout testing. Also, the zeta potential during the preparation at a normal pH of 6.5 was -41.9 ± 1.9 and -49.0 ± 2.5 mV (measured three times, $n = 3$) because gum Arabic possessed a negative charge, as shown in Fig. 4c and d. The different sizes, distribution, and zeta potential values of the made Cu and Zn silicate NPs are listed in Table 1.

The reliable part of this study is that the NPs produced are very stable over a long time because gum Arabic helps protect them, improving them for possible long-term use in cosmetics, medicine, biomedical fields, and plant protection.[49–52]

According to the literature,[53] the FTIR results showed absorption peaks at 3291 cm^{-1} (caused by –OH), 2985 cm^{-1} (caused by symmetric and asymmetric –CH vibration), 1642 cm^{-1} (caused by –COOH), 1462 cm^{-1} (caused by the symmetrical stretching of uronic acid by carboxylic groups), 1066 cm^{-1} (perhaps caused by arabinogalactan), and 890.0 cm^{-1} (caused by galactose 1–4 linkage and mannose 1–6 linkage). The metal NP spectra show the same peaks, suggesting that gum Arabic was effective at capping. In addition, the arabinogalactan peak lost its doublet, and the galactose/mannose peak became less noticeable. Furthermore, a prominent peak was seen at 715.25 cm^{-1}, which might be the result of metal nanoparticles reacting and joining forces with hydroxyl groups to produce metal–O.[54] According to the findings of El-Batal *et al.*,[53] the absence of noise and other unknown peaks demonstrated the purity of the synthesized material. Furthermore, all of the peaks fell within the same wavenumbers, indicating that the synthesized NPs were conjugated and incorporated into the major functional groups of the stabilizer gum Arabic in a comparable manner.[52]

Table 1 PSD, PDI, and zeta potential values of the synthesized Cu silicate and Zn silicate NPs

Nanocomposite	PSD (nm)	PDI	Zeta potential (mV)
Cu silicate NPs	219.4 ± 2.0	0.86	-41.9 ± 1.9
Zn silicate NPs	192.0 ± 1.7	0.81	-49.0 ± 2.5

3.2. Antimicrobial activity of Cu silicate and Zn silicate NPs

Cu and Zn silicate nanoparticles were tested for their ability to kill bacteria and Candida using an agar-disc diffusion method. According to Table 2, and Fig. 5, the Cu silicate NPs created a 27.0 mm ZOI against *S. aureus* with MIC of 39.062 µg mL^{-1}, followed by a 25.0 mm ZOI against *C. albicans* with MIC of 19.53 µg mL^{-1} and a 19.0 mm ZOI against *E. agglomerans* with MIC of 19.53 µg mL^{-1}. This value indicates the antibacterial efficacy of the Cu silicate NPs.

On the other hand, Cu silicate NPs had an 18.0 mm activity against *P. aeruginosa* and *K. pneumonia*. However, as shown in Table 2, Zn silicate NPs work better against *S. aureus* (41.0 mm ZOI, and 19.53 µg per mL MIC), then *C. albicans* (30.0 mm ZOI, and 9.765 µg per mL MIC), *E. agglomerans* (29.0 mm ZOI, and 39.062 µg per mL MIC), and *S. epidermidis* (28.0 mm ZOI, and 19.53 µg per mL MIC). In contrast, *K. pneumoniae*, *P. aeruginosa*, and *E. coli* were found to be 26.0 mm ZOI, and 9.765 µg per mL MIC, 25.0 mm ZOI, and 9.765 µg per mL MIC, and 21.0 mm ZOI, and 19.53 µg per mL MIC, respectively.

The mechanism of action of Cu and Zn silicate NPs is electrostatic interaction. Reactive oxygen species (ROS) and oxidative stress are produced, which harm cell membranes, interfere with proteins and enzymes, block signal transmission, damage genes, and prevent proteins from keeping balance in the body (disruption of the electronic transport chain).[55,56]

Zhang, Jiang, Ding, Povey, and York,[57] say that the roughness of the ZnO NPs' exterior surface may further contribute to their efficiency by causing damage to the cell wall and allowing them to enter the plasma membrane, where they kill bacteria. Inorganic metal oxide NPs have several traits, such as a small size and a high surface-to-volume ratio. When interacting with certain infectious microorganisms, like bacteria, they can exhibit unique and significant behaviors.[58]

Inorganic NPs can be used in a variety of medical applications because of their special qualities. Furthermore, they lessen the efficiency of conventional antibiotics and their potential for use as treatments by making certain bacteria more resistant to them.[59] They kept the right physical and chemical traits, like a unique way of interacting, which helped them work better against more harmful bacteria and yeast and boosted their antibacterial activity, unlike most natural and synthetic antimicrobials.[60]

Nevertheless, it is unclear how Cu silicate and Zn silicate NPs work as an antibiotic. The pathogenic bacteria's combination of nano-silica and an alkaline inclination demonstrated how the antibacterial activity operated.[61] Using incredibly intricate processes, ROS such as superoxide anion; O_2^- were released.[62] According to some theories, Cu and Zn silicate NPs may alter the way that microorganisms form films, how quickly they can cross membranes, and how oxidative stress genes function in response to H_2O_2 generation.[63]

3.3. Antibiofilm activity of the synthesized Cu silicate and Zn silicate NPs

Certain pathogenic microorganisms have been found to produce exopolysaccharide molecules that can form biofilms.[64] The bacteria most vulnerable to Cu silicate NPs, *C. albicans*, which are unicellular fungi, *S. epidermidis*, which is an example of Gram-positive bacteria, and *P. aeruginosa*, which is an example of Gram-negative bacteria, were grown using tube techniques to evaluate the biofilm formation, as shown in Fig. 6.

Using a UV-Vis spectrophotometer set to 570.0 nm, we measured how much the microorganisms that create bacterial biofilms were inhibited. To check how much the colored (CV) bacterial biofilm could be dissolved in ethanol and to see how much light it absorbed, we measured its optical density. Table 3 displays the percentage of inhibition of the three chosen bacterial and yeast strains' capacity to form biofilms. The highest level of inhibition, 89.94%, was seen in *P. aeruginosa* when treated with 19.53 µg per mL Cu silicate NPs. Next in line were *C. albicans* (86.75% inhibition) and *S. epidermidis* (73.78%) with 39.062 µg per mL Cu silicate NPs.

In contrast, as shown in Fig. 7, the bacteria that were most affected by Zn silicate NPs were tested using tube methods to check how well they formed biofilms. The greatest reduction in growth (88.15%) was noted in *P. aeruginosa* treated having 9.765 µg per mL Zn silicate NPs, followed by *C. albicans* (79.31%) also treated with 9.765 µg per mL Zn silicate NPs, and *S. epidermidis* (66.91%) treated with 19.53 µg per mL Zn silicate NPs, as shown in Table 3.

By entering the film and destroying the microbial cells that aid in the biofilm's growth, NPs can continue to have an impact on the formed biofilm in the second stage. Therefore, we believe that NP-based antibiofilm coatings could serve as probes for biofilm removal, imaging, and treatment. Their low toxicity and wide range of activity are additional benefits. Semiconductor

Table 2 Antimicrobial activity of Cu silicate and Zn silicate NPs (mm) and MIC (µg mL^{-1})

| Pathogenic microbes	ZOI of Cu silicate NPs (mm)	MIC of Cu silicate NPs (µg mL^{-1})	ZOI of Zn silicate NPs (mm)	MIC of Zn silicate NPs (µg mL^{-1})	Standard antibiotics (streptomycin, and nystatin)
Klebsiella pneumoniae	18.0 ± 0.22	39.062	26.0 ± 0.18	9.765	Nil
Enterobacter agglomerans	19.0 ± 0.18	78.125	29.0 ± 0.33	39.062	16.0 ± 0.50
Escherichia coli	14.0 ± 0.23	78.125	21.0 ± 0.20	19.53	13.0 ± 0.22
Pseudomonas aeruginosa	18.0 ± 0.20	19.53	25.0 ± 0.22	9.765	9.0 ± 0.23
Staphylococcus epidermidis	17.0 ± 0.22	39.062	28.0 ± 0.19	19.53	20.0 ± 0.20
Staphylococcus aureus	27.0 ± 0.19	39.062	41.0 ± 0.50	19.53	Nil
Candida albicans	25.0 ± 0.50	19.53	30.0 ± 0.22	9.765	Nil
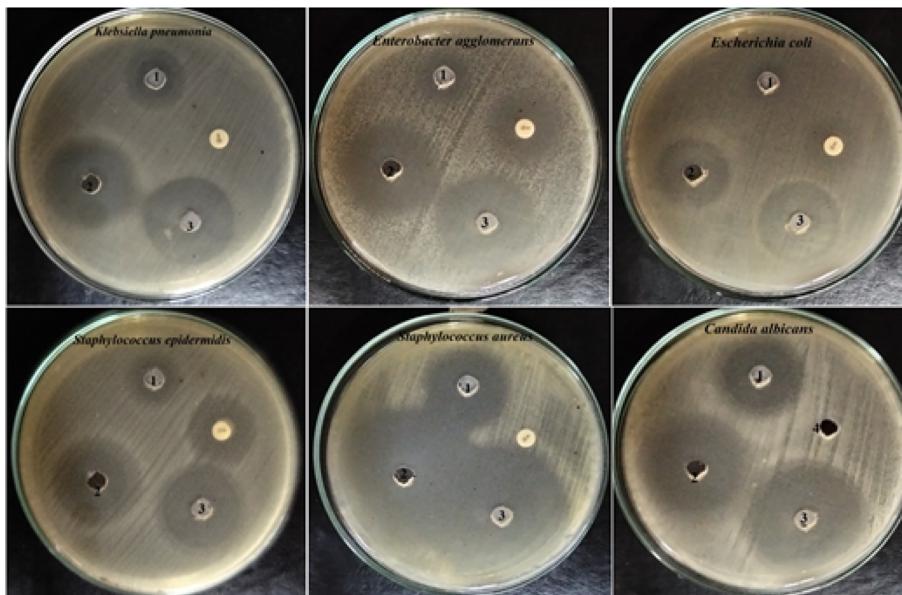
Fig. 5 Antimicrobial activity of Cu and Zn silicate NPs against some tested pathogenic microbes, where 1 = Cu silicate, 2 = Zn silicate, and 3 = their combination.

nanoparticles may be used to detect and observe inhibitory processes.[65]

3.4. Growth curve assay

Analysis was done on how the synthesized Cu silicate and Zn silicate NPs affected the kinetic development (growth) of *C. albicans*, *P. aeruginosa*, and *S. epidermidis*, which all grow quickly in the control sample, as shown in Fig. 8. As can be shown in Fig. 8a, *C. albicans* expanded quickly in the control sample, peaking at 2.744 nm for the optical density at $\lambda = 600$ nm (OD_{600}). The OD_{600} value of Cu silicate NPs was found to be 1.733, and Zn silicate NPs at 1.829 indicating a repressive effect on the development of *C. albicans*.

In the same way, Fig. 8b shows that *P. aeruginosa* grew rapidly in the untreated sample, reaching a high of 2.223 nm in the OD_{600} value. Additionally, the OD_{600} value (1.603, and 1.849 nm) after treatment with Cu silicate, and Zn silicate NP, respectively indicates that *P. aeruginosa* growth was reduced. Finally, it is evident from Fig. 8c that *S. epidermidis* developed quickly in the untreated sample, peaking at 2.431 nm in terms of its OD_{600} value. Additionally, the OD_{600} value of 1.234, and 1.123 nm after treating with Cu silicate, and Zn silicate NPs, respectively indicates that *S. epidermidis* growth was reduced.

In general, earlier research has examined the production of ROS by photogeneration on the surface of ZnO NPs.[66] Cu silicate and Zn silicate NPs can destroy bacteria while shielding other cells by generating ROS, which oxidize proteins, damage DNA, and peroxide lipids.

Additionally, the membranes of *P. aeruginosa* and *S. epidermidis* possessed a negative charge, and the metal ion generated by Cu silicate, and Zn silicate (Cu^{2+} and Zn^{2+}) have a positive charge. Thus, the synthesized NPs directly impact bacterial cell collapse, protein denaturation, and DNA

replication. The limited mobility of the bacterial cell membrane may be the cause of the increased susceptibility of bacteria to Cu silicate and Zn silicate NPs. Cu silicate and Zn silicate NPs probably interact with bacteria more easily due to their size, shape, and surface charge.

After 80 minutes of exposure to UV radiation, NPs broke down the *E. coli* membrane, proving that disinfection was effective.[67] Many NPs demonstrated potential as antibacterial agents that are effective toward a variety of bacteria like *E. coli*, and *S. aureus*, according to many publications.

3.5. Microbial protein leakage investigation

Using the Bradford technique, we determined the amounts of protein permeability in the treated solutions of *P. aeruginosa*, *C. albicans*, and *S. epidermidis*.[68] The amount of protein from *P. aeruginosa*, *C. albicans*, and *S. epidermidis* that was removed is directly related to the amount of Cu silicate, and Zn silicate NPs used, as shown in Fig. 9a and b. After treatment with 1.0 mg per mL Cu silicate NPs, the amounts *C. albicans*, *P. aeruginosa*, and *S. epidermidis* were 101.34, 80.34, and 110.32 μg mL^{-1}, respectively Fig. 9a. In the same manner, after treatment with 1.0 mg per mL Zn silicate NPs, the amounts *C. albicans*, *P. aeruginosa*, and *S. epidermidis* were 90.23, 60.46, and 88.32 μg mL^{-1}, respectively Fig. 9b. This illustrates how the tested microorganisms' membranes developed holes that allowed the proteins to escape the microbial cytoplasm and display the antibacterial behavior of the synthesized Cu silicate, and Zn silicate NPs.

The results showed that using Cu silicate, and Zn silicate NPs together made it easier for microbial membranes to break down and caused more leakage than using Cu silicate, and Zn silicate NPs by themselves. The metal helps make bacterial membranes
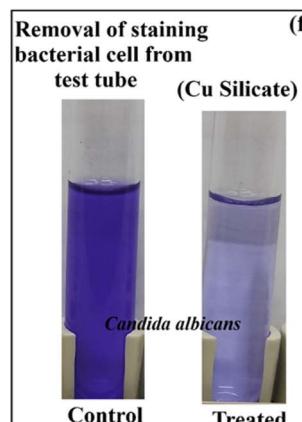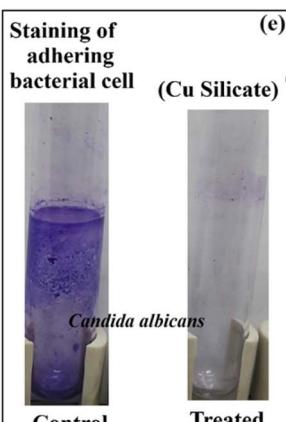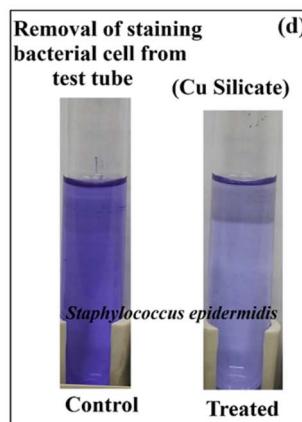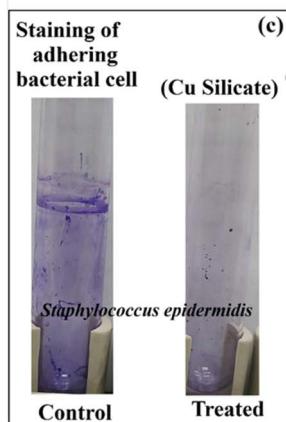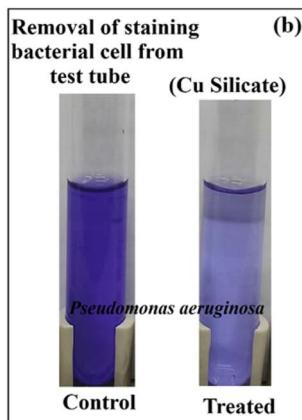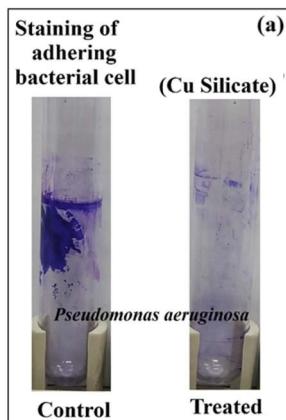
Fig. 6 Cu silicate NPs' antibiofilm activity against *P. aeruginosa* (a and b), *S. epidermidis* (c and d), and *C. albicans* (e and f) where the adherent bacterial cell's staining with Crystal Violet stain, and finally crystal violet's decolorization *via* ethanol.
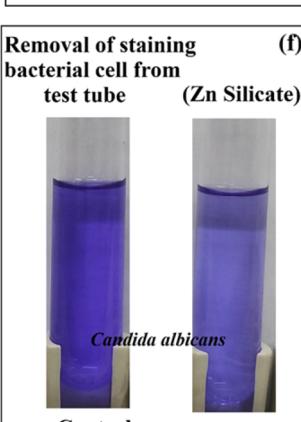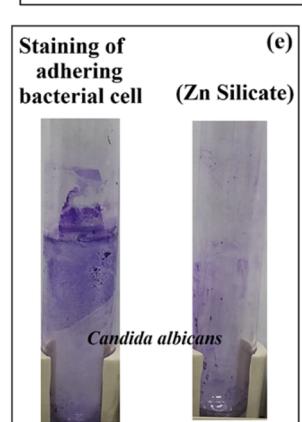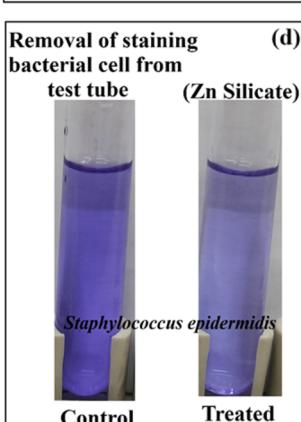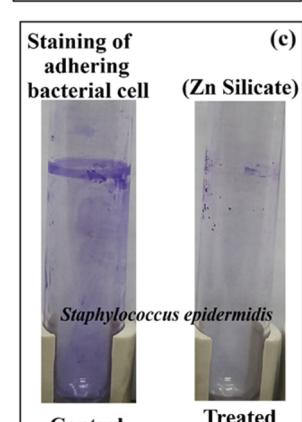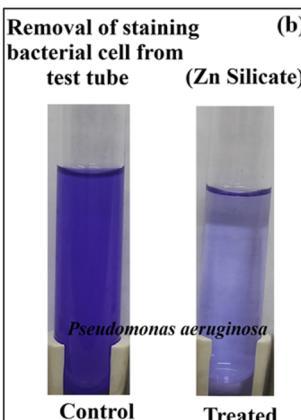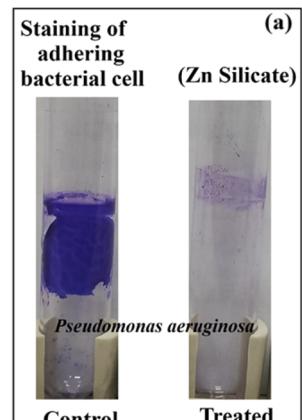
Fig. 7 Zn silicate NPs' antibiofilm activity against *P. aeruginosa* (a and b), *S. epidermidis* (c and d), and *C. albicans* (e and f) where the adherent bacterial cell's staining with Crystal Violet stain, and finally crystal violet's decolorization *via* ethanol.

Table 3 The antibiofilm activity of the synthesized Cu silicate and Zn silicate NPs by test tube methods

| Microbial isolates	O.D of C.V stain at 570.0 nm (control)	O.D of C.V stain at 570.0 nm (treated)		Inhibition %	
		Cu silicate NPs	Zn silicate NPs	Cu silicate NPs	Zn silicate NPs
Pseudomonas aeruginosa	2.843 ± 0.1344	0.279 ± 0.0200	0.337 ± 0.0211	89.94	88.15
Staphylococcus epidermidis	0.982 ± 0.0983	0.274 ± 0.0212	0.325 ± 0.0165	73.78	66.91
Candida albicans	1.986 ± 0.1251	0.320 ± 0.0198	0.411 ± 0.0200	86.75	79.31
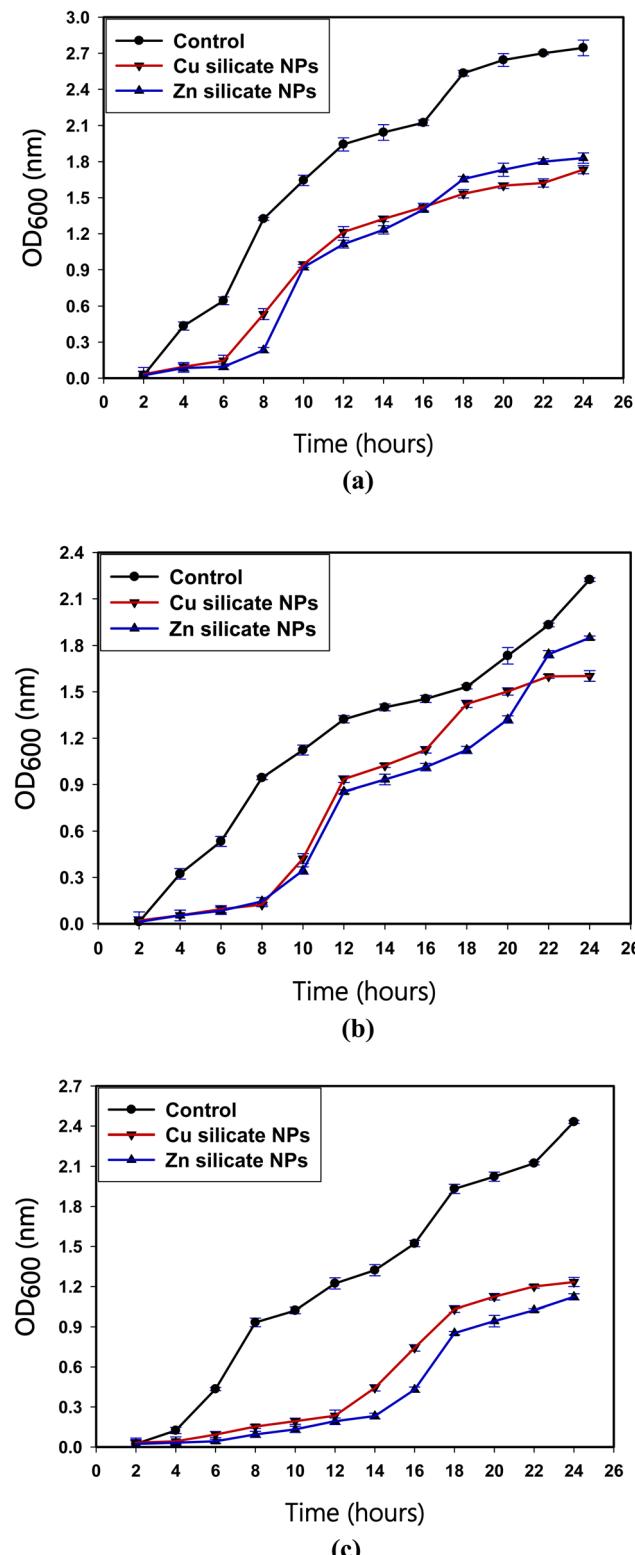
Fig. 8 Effect of Cu silicate and Zn silicate NPs on the kinetics of (a) *C. albicans* (b) *P. aeruginosa* and (c) *S. epidermidis* growth with time intervals.

more permeable, leading to protein leakage, which is the key reason it stops bacteria from growing.
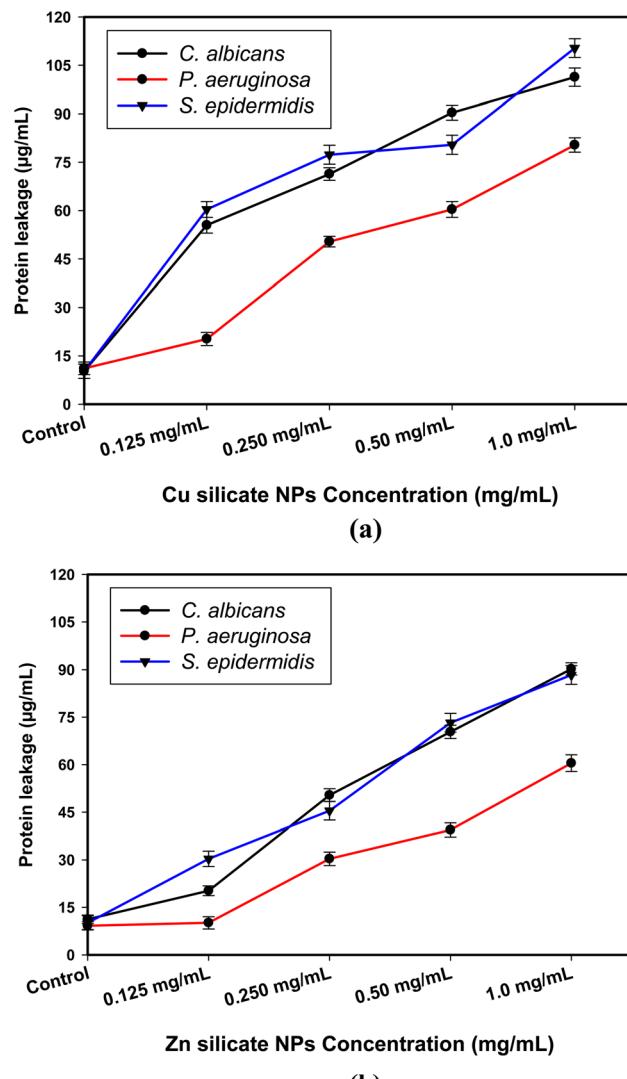

Fig. 9 The effect of Cu silicate NPs (a), and Zn silicate NPs (b) on the protein leakage from *C. albicans*, *P. aeruginosa*, and *S. epidermidis* cell membranes.

Similar results after NP treatment are described in similar research, such as,[69,70] which has been shown that the concentration affects how bacteria lose their outer membrane and leak their internal parts. Paul *et al.*,[71] claim that the differences in electric conductivity caused the changes in how easily bacteria's membranes let substances through. The protein leakage test is one of the most crucial techniques for figuring out a microbe's skeletal strength. The final conversion of the leak into typical microbial damage and the loss of cell components led to cell collapse.

4 Conclusion and future perspectives

The current work effectively synthesized Cu silicate and Zn silicate NPs using an environmentally friendly method. The generated NPs exhibit promising nanomaterial properties, including a uniform, spherical surface, a multidimensional

structure, and a homogenous size. According to the study of how microorganisms multiply and grow (growth curve), *C. albicans* grew rapidly in the control sample, reaching a maximum of 2.744 nm for the optical density at $\lambda = 600$ nm (OD_{600}). Cu silicate NPs had an OD_{600} value of 1.733, whereas Zn silicate NPs had an OD_{600} value of 1.829, suggesting that they had a suppressive impact on *C. albicans* development. The highest level of biofilm inhibition (89.94%) was observed in *P. aeruginosa* when treated with 19.53 μg per mL Cu silicate NPs. *C. albicans* showed an 86.75% reduction in biofilm creation, while *S. epidermidis* had a 73.78% reduction in biofilm when treated with 39.062 μg per mL Cu silicate NPs. The membrane leakage experiment was applied to investigate the mechanism of the antibacterial action. The amounts of protein released from *C. albicans*, *P. aeruginosa*, and *S. epidermidis* were 101.34, 80.34, and 110.32 μg mL^{-1}, respectively, after being treated with 1.0 mg per mL Cu silicate NPs. In the same way, the amounts of protein released from *C. albicans, P. aeruginosa*, and *S. epidermidis* were 90.23, 60.46, and 88.32 μg mL^{-1}, respectively, after being treated with 1.0 mg per mL Zn silicate NPs. This study shows how microbial membrane may form holes that allow proteins to escape from microbial cytoplasm and highlights the antibacterial properties of the synthesized Cu silicate and Zn silicate NPs. To further understand how effectively it contrasts with other antibiotics, future studies must look at how it interacts with bacterial cell walls and how it influences antibiotic resistance. Finally, some characterization methods (such as Raman, XRD, and FTIR) must be performed to confirm the purity, crystallinity and the chemical interactions between gum Arabic function groups and the synthesized NPs.

Author contributions

Conceptualization of the study: A. A. Q., I. E., F. A. N., A. A. E., G. S. E., and A. I. E.; methodology: A. A. Q., I. E., F. A. N., A. A. E., G. S. E., and A. I. E.; data acquisition: A. A. Q., I .E., F. A. N., A. A. E., G. S. E., and A. I. E.; analysis and interpretation of data: A. A. Q., I. E., F. A. N., A. A. E., G. S. E., and A. I. E.; drafting of the manuscript: A. A. Q., I. E., F. A. N., A. A. E., G. S. E., and A. I. E.; critical revision of the manuscript: A. A. Q., I. E., F. A. N., A. A. E., G. S. E., and A. I. E.; all authors have approved the final manuscript.

Conflicts of interest

No conflict of interests.

Data availability

The data sets used and analyzed during the current study are available from the corresponding author upon reasonable request.

Acknowledgements

References

1 S. K. Ahmed, S. Hussein, K. Qurbani, R. H. Ibrahim, A. Fareeq, K. A. Mahmood and M. G. Mohamed, *J. Med. Surg. Public Health*, 2024, **2**, 100081.

2 R. Biselli, R. Nisini, F. Lista, A. Autore, M. Lastilla, G. De Lorenzo, M. S. Peragallo, T. Stroffolini and R. D'Amelio, *Biomedicines*, 2022, **10**, 2050.

3 G. S. El-Sayyad, *Discovery Bact.*, 2024, **1**, 2.

4 L. S. Platt and A. Mahmoudi, *Technology*, 2024, **8**, 70–82.

5 A. Mirzapoor and E. Ghashghaee, *Inorg. Chem. Commun.*, 2023, **153**, 110840.

6 H.-N. Barad, H. Kwon, M. Alarcón-Correa and P. Fischer, *ACS Nano*, 2021, **15**, 5861–5875.

7 S. Mourdikoudis, R. M. Pallares and N. T. K. Thanh, *Nanoscale*, 2018, **10**, 12871–12934.

8 N. Baig, I. Kammakakam and W. Falath, *Mater. Adv.*, 2021, **2**, 1821–1871.

9 S. Ghosh, S. K. Sharma, S. Rana, T. S. Khan, T. Sasaki, S. S. Acharyya and R. Bal, *ACS Appl. Nano Mater.*, 2023, **6**, 17668–17680.

10 N. T. K. Thanh, N. Maclean and S. Mahiddine, *Chem. Rev.*, 2014, **114**, 7610–7630.

11 M. Shaaban and A. M. El-Mahdy, *IET Nanobiotechnol.*, 2018, **12**, 741–747.

12 B. Mubeen, A. N. Ansar, R. Rasool, I. Ullah, S. S. Imam, S. Alshehri, M. M. Ghoneim, S. I. Alzarea, M. S. Nadeem and I. Kazmi, *Antibiotics*, 2021, **10**, 1473.

13 M. Xie, M. Gao, Y. Yun, M. Malmsten, V. M. Rotello, R. Zboril, O. Akhavan, A. Kraskouski, J. Amalraj and X. Cai, *Angew. Chem., Int. Ed.*, 2023, **62**, e202217345.

14 A. Khezerlou, M. Alizadeh-Sani, M. Azizi-Lalabadi and A. Ehsani, *Microb. Pathogen.*, 2018, **123**, 505–526.

15 S. Shouket, J. Khan, R. Batool, A. Sarwar, T. Aziz, M. Alhomrani, A. S. Alamri, M. Y. Sameeh and F. Z. Filimban, *Food Res. Int.*, 2023, **169**, 112940.

16 N. Babayevska, Ł. Przysiecka, I. Iatsunskyi, G. Nowaczyk, M. Jarek, E. Janiszewska and S. Jurga, *Sci. Rep.*, 2022, **12**, 8148.

17 A. Biswas, U. Kar and N. R. Jana, *Phys. Chem. Chem. Phys.*, 2022, **24**, 13965–13975.

18 R. K. Dutta, B. P. Nenavathu and S. Talukdar, *Colloids Surf., B*, 2014, **114**, 218–224.

19 R. K. Dutta, B. P. Nenavathu, M. K. Gangishetty and A. Reddy, *J. Environ. Sci. Health, Part A*, 2013, **48**, 871–878.

20 R. Zhang, Z. Chen, Y. Li, D. Chen, T. Wang, B. Wang, Q. Zhou, S. Cheng, D. Xu and X. Wang, *J. Mater. Sci. Technol.*, 2024, **192**, 173–189.

21 C. Zhang, X. Wang, J. Du, Z. Gu and Y. Zhao, *Adv. Sci.*, 2021, **8**, 2002797.

22 M. Li, S. Pokhrel, X. Jin, L. Mädler, R. Damoiseaux and E. M. Hoek, *Environ. Sci. Technol.*, 2011, **45**, 755–761.

23 B. N. Dole, V. D. Mote, V. R. Huse, Y. Purushotham, M. K. Lande, K. M. Jadhav and S. S. Shah, *Curr. Appl Phys.*, 2011, **11**, 762–766.

24 N. Verma, D. Pathak, K. Kumar, K. Jeet, S. Nimesh, L. Loveleen, S. Kumar and N. Thakur, *Mater. Chem. Phys.*, 2025, **333**, 130422.

25 Z. Li, Y. Z. Khimyak and A. Taubert, Lessons from a "Failed" Experiment: Zinc Silicates with Complex Morphology by Reaction of Zinc Acetate, the Ionic Liquid Precursor (ILP) Tetrabutylammonium Hydroxide (TBAH), and Glass, *Materials*, 2008, **1**(1), 3–24, DOI: **10.3390/ma1010003**.

26 J. R. Rischbieth and F. Marson, *Nature*, 1961, **192**, 748.

27 S. Bawaked and K. Narasimharao, *Sci. Rep.*, 2020, **10**, 518.

28 P. S. Shinde, P. S. Suryawanshi, K. K. Patil, V. M. Belekar, S. A. Sankpal, S. D. Delekar and S. A. Jadhav, *J. Compos. Sci.*, 2021, **5**, 75.

29 C. Calabrese, V. L. Parola, S. Cappello, A. Visco, C. Scolaro and L. F. Liotta, *Nanomaterials*, 2022, **12**, 2371.

30 H. A. El-Wahab, E. K. Alenezy, N. Omer, M. A. Abdelaziz, R. Jame, S. A. Alshareef and M. Owda, *Sci. Rep.*, 2024, **14**, 24413.

31 R. G. Elfadel, H. M. Refat, H. A. El-Wahab, S. S. Salem, M. Owda and M. Abdel Reheim, *Sci. Rep.*, 2023, **13**, 7268.

32 A. Nayl, A. Abd-Elhamid, A. A. Aly and S. Bräse, *RSC Adv.*, 2022, **12**, 13706–13726.

33 G. Voicu, O. Oprea, B. Vasile and E. Andronescu, *Dig. J. Nanomater. Biostruct.*, 2013, **8**, 667–675.

34 F. Hemmati, R. Salehi, R. Ghotaslou, H. S. Kafil, A. Hasani, P. Gholizadeh and M. A. Rezaee, *Int. J. Biol. Macromol.*, 2020, **163**, 2248–2258.

35 G. D. Christensen, W. A. Simpson, A. L. Bisno and E. H. Beachey, *Infect. Immun.*, 1982, **37**, 318–326.

36 W. Huang, J.-Q. Wang, H.-Y. Song, Q. Zhang and G.-F. Liu, *Asian Pac. J. Trop. Med.*, 2017, **10**, 663–669.

37 H. Agarwal, A. Nakara, S. Menon and V. Shanmugam, *J. Drug Delivery Sci. Technol.*, 2019, **53**, 101212.

38 A. M. Brown, *Comput. Methods Programs Biomed.*, 2005, **79**, 89–95.

39 E. Castro-Longoria, A. R. Vilchis-Nestor and M. Avalos-Borja, *Colloids Surf., B*, 2011, **83**, 42–48.

40 M. Bouatrous, F. Bouzerara and Q. Bizot, *J. Inorg. Organomet. Polym. Mater.*, 2024, **34**, 1931–1943.

41 M. Nissen, R. Förster, T. Wieduwilt, A. Lorenz, S. Jiang, W. Hauswald and M. A. Schmidt, *Small*, 2022, **18**, 2202024.

42 S. S. Salem, *Appl. Biochem. Biotechnol.*, 2022, **194**, 1898–1910.

43 T. G. Souza, V. S. Ciminelli and N. D. S. Mohallem, *J. Phys.:Conf. Ser.*, 2016, **733**, 012039.

44 M. I. Magzoub, I. A. Hussein, M. S. Nasser, M. Mahmoud, A. S. Sultan and A. Benamor, *J. Dispersion Sci. Technol.*, 2020, **41**, 817–827.

45 V. Shulkin and A. Y. Strukov, *Russ. J. Pac. Geol.*, 2020, **14**, 378–386.

46 N. Farkas and J. A. Kramar, *J. Nanopart. Res.*, 2021, **23**, 120.

47 S. R. Falsafi, H. Rostamabadi, E. Assadpour and S. M. Jafari, *Adv. Colloid Interface Sci.*, 2020, **280**, 102166.

48 S. Samal, *Powder Technol.*, 2020, **366**, 43–51.

49 K. M. Khazaei, S. Jafari, M. Ghorbani and A. H. Kakhki, *Carbohydr. Polym.*, 2014, **105**, 57–62.

50 T. Moschakis, B. S. Murray and C. G. Biliaderis, *Food Hydrocolloids*, 2010, **24**, 8–17.

51 R. Sukhotu, S. Guo, J. Xing, Q. Hu, R. Wang, X. Shi, K. Nishinari, Y. Fang and S. Guo, *LWT–Food Sci. Technol.*, 2016, **68**, 432–438.

52 A. I. El-Batal, N. M. Balabel, M. S. Attia and G. S. El-Sayyad, *J. Cluster Sci.*, 2020, **31**, 1021–1040.

53 A. I. El-Batal, M. Abd Elkodous, G. S. El-Sayyad, N. E. Al-Hazmi, M. Gobara and A. Baraka, *Int. J. Biol. Macromol.*, 2020, **165**, 169–186.

54 A. Ashour, A. I. El-Batal, M. A. Maksoud, G. S. El-Sayyad, S. Labib, E. Abdeltwab and M. El-Okr, *Particuology*, 2018, **40**, 141–151.

55 P. V. Baptista, M. P. McCusker, A. Carvalho, D. A. Ferreira, N. M. Mohan, M. Martins and A. R. Fernandes, *Front. Microbiol.*, 2018, **9**, 1441.

56 N. Arora, K. Thangavelu and G. N. Karanikolos, *Front. Chem.*, 2020, **8**, 412.

57 L. Zhang, Y. Jiang, Y. Ding, M. Povey and D. York, *J. Nanopart. Res.*, 2007, **9**, 479–489.

58 S. L Palencia, A. M Buelvas and M. S. Palencia, *Curr. Chem. Biol.*, 2015, **9**, 10–22.

59 Y. Xia, Y. Zhou and Z. Tang, *Nanoscale*, 2011, **3**, 1374–1382.

60 A. H. Hashem, E. Saied, O. M. Ali, S. Selim, S. K. Al Jaouni, F. M. Elkady and G. S. El-Sayyad, *Appl. Biochem. Biotechnol.*, 2023, **195**, 5753–5776.

61 M. Dryden, *Int. J. Antimicrob. Agents*, 2018, **51**, 299–303.

62 A. H. Hashem and G. S. El-Sayyad, *Biomass Convers. Biorefin.*, 2024, **14**, 20345–20357.

63 A. Nawaz, A. Farhan, F. Maqbool, H. Ahmad, W. Qayyum, E. Ghazy, A. Rahdar, A. M. Díez-Pascual and S. Fathi-karkan, *J. Mol. Struct.*, 2024, **138545**.

64 M. A. Ansari, H. M. Khan, A. A. Khan, S. S. Cameotra and R. Pal, *Appl. Nanosci.*, 2014, **4**, 859–868.

65 E. Priyadarshini, K. Rawat and H. B. Bohidar, in *Nonmagnetic and Magnetic Quantum Dots*, IntechOpen, 2017.

66 A. Joe, S.-H. Park, D.-J. Kim, Y.-J. Lee, K.-H. Jhee, Y. Sohn and E.-S. Jang, *J. Solid State Chem.*, 2018, **267**, 124–133.

67 Y. Xu, Q. Liu, M. Xie, S. Huang, M. He, L. Huang, H. Xu and H. Li, *J. Colloid Interface Sci.*, 2018, **528**, 70–81.

68 N. J. Kruger, *The Protein Protocols Handbook*, 2002, pp. 15–21.

69 S. Rajesh, V. Dharanishanthi and A. V. Kanna, *J. Exp. Nanosci.*, 2015, **10**, 1143–1152.

70 Z. Azam, A. Ayaz, M. Younas, Z. Qureshi, B. Arshad, W. Zaman, F. Ullah, M. Q. Nasar, S. Bahadur and M. M. Irfan, *Microb. Pathogen.*, 2020, **144**, 104188.

71 D. Paul, S. Maiti, D. P. Sethi and S. Neogi, *Adv. Powder Technol.*, 2021, **32**, 131–143.